Two conformations of the integrin A-domain (I-domain): a pathway for activation?

Jie-Oh Lee[1], Laurie Anne Bankston[1†], M Amin Arnaout[2*] and Robert C Liddington[1†*]

[1]Dana-Farber Cancer Institute and Dept. of Biological Chemistry and Molecular Pharmacology, Harvard Medical School, 44 Binney St, Boston, MA 02115, USA and [2]Leukocyte Biology and Inflammation Program, Nephrology Division, Dept. of Medicine, Massachusetts General Hospital and Harvard Medical School, Charlestown, MA 02129, USA

Background: Integrins are plasma membrane proteins that mediate adhesion to other cells and to components of the extracellular matrix. Most integrins are constitutively inactive in resting cells, but are rapidly and reversibly activated in response to agonists, leading to highly regulated cell adhesion. This activation is associated with conformational changes in their extracellular portions, but the nature of the structural changes that lead to a change in adhesiveness is not understood. The interactions of several integrins with their extracellular ligands are mediated by an A-type domain (generally called the I-domain in integrins). Binding of the I-domain to protein ligands is dependent on divalent cations. We have described previously the structure of the I-domain from complement receptor 3 with bound Mg^{2+}, in which the glutamate side chain from a second I-domain completes the octahedral coordination sphere of the metal, acting as a ligand mimetic.

Results: We now describe a new crystal form of the I-domain with bound Mn^{2+}, in which water completes the metal coordination sphere and there is no equivalent of the glutamate ligand. Comparison of the two crystal forms reveals a change in metal coordination which is linked to a large (10 Å) shift of the C-terminal helix and the burial of two phenylalanine residues into the hydrophobic core of the Mn^{2+} form. These structural changes, analogous to those seen in the signal-transducing G-proteins, alter the electrophilicity of the metal, reducing its ability to bind ligand-associated acidic residues, and dramatically alter the surface of the protein implicated in binding ligand.

Conclusions: Our observations provide the first atomic resolution view of conformational changes in an integrin domain, and suggest how these changes are linked to a change in integrin adhesiveness. We propose that the Mg^{2+} form represents the conformation of the domain in the active state and the Mn^{2+} form the conformation in the inactive state of the integrin.

Structure 15 December 1995, **3**:1333–1340

Key words: activation, A-domain, crystal structure, I-domain, integrin, metal binding

Introduction

The integrin family of cell-adhesion molecules are αβ heterodimers with a generally conserved structure [1]. So far, 16 distinct α subunits (with ~1000 residues) have been identified that pair with eight different β subunits (~750 residues). Electron microscopy indicates that integrins have an extracellular globular 'head' (~100 Å diameter) comprising the N-terminal portion of both subunits, followed by a long 'stalk' (~100 Å) between the globular head and the membrane-spanning helices, and a short C-terminal cytoplasmic 'tail' for each subunit.

Biochemical and biophysical probes have shown that activation of integrins to an adhesion-promoting state involves conformational changes in the extracellular domains. Thus, fluorescence energy transfer experiments show that the integrin $\alpha_{IIb}\beta_3$ changes shape on activation [2], and there is also a marked change in proteolytic sensitivity, consistent with a change of shape and/or rigidity [3]. Furthermore, monoclonal antibodies have been described that discriminate between active and inactive states (reviewed in [4–6]). Allostery within the extracellular domains has been vividly demonstrated by electron miscroscopic images of integrins with both activating antibodies and ligands bound, separated by a distance of 160 Å [7]. However, the nature of the conformational changes that lead to a change in adhesiveness is not known.

Seven integrin α subunits contain a ~190-residue sequence near their N terminus that is homologous to the A-domains of von Willebrand factor, and is generally called the I-domain in integrins. This domain plays a major role in ligand binding [8–14], and undergoes conformational changes in response to receptor activation [14–16]. We have previously proposed that a conserved region found in all β subunits, and implicated in ligand binding, also adopts an A-type fold [17].

The β_2 integrins are a subfamily of integrins found exclusively on leukocytes [18]. One of them, complement receptor 3 (CR3; also known as CD11b/CD18, $\alpha_M\beta_2$ or Mac-1), is the major integrin of phagocytic cells, and is required for phagocytosis and the stable adhesion of leukocytes to endothelium and the subsequent migration into inflamed organs. These functions are mediated through binding to several physiologic ligands including iC3b (the major complement C3 opsonin),

*Corresponding authors. †Present address: Department of Biochemistry, University of Leicester, University Road, Leicester LE1 7RH, UK.

ICAM-1 (CD54), and the coagulation factor fibrinogen. The recombinant I-domain from CR3 has many of the binding functions of the intact receptor, and ligand binding is dependent on divalent cations. We have previously determined its structure from crystals grown in the presence of Mg^{2+} [17]. It adopts a classic 'dinucleotide-binding' or 'Rossmann' fold, and contains an unusual Mg^{2+} coordination site at its surface, which we call the metal-ion-dependent adhesion site (MIDAS) motif. Point mutations in the MIDAS motif abrogate cation binding and binding to many protein ligands [8–10,17]. In the Mg^{2+}-containing I-domain crystal, one of the coordinating ligands is the glutamate side chain from another I-domain molecule, and we have proposed that this interaction is a mimic of a natural integrin–ligand interaction, because all known integrin ligands contain acidic residues as a key feature of their binding motifs [19].

Here we describe a new crystal form of the I-domain, grown in the presence of Mn^{2+}, in which the domain is 'unliganded', and compare it with the previously described 'liganded' structure grown in the presence of Mg^{2+}. The two structures display large differences, and we propose that they represent the conformations of the domain that exist in the active and inactive states of the integrin.

Results and discussion

Two crystal structures of the I-domain

The I-domain adopts the dinucleotide-binding or Rossmann fold, with seven α helices (labelled α1–α7) surrounding a mostly parallel β sheet (labelled βA–βF; Fig. 1a). The MIDAS motif is located in a crevice at the top of the sheet. The motif, conserved in many members of the A-domain superfamily, comprises a DxSxS sequence (residues 140–144; single-letter code; where x is any amino acid) from the βA–α1 loop, Thr209 from the α3–α4 loop and Asp242 from the βD–α5 loop. Crystallization of the domain in a minimal concentration of Mn^{2+} produced a crystal form different from that previously obtained in an excess of Mg^{2+} [17]. We determined the Mn^{2+} I-domain structure by molecular replacement and refined the model at 2.0 Å resolution (Fig. 1b). About two-thirds of the molecule has a very similar structure in both crystal forms: the central β sheet (except for βF) and the α helices (except for α1, α6 and α7) can be closely superimposed; residues 132–140, 167–241 and 245–265 overlap with a root mean square (rms) difference for main-chain atoms of 0.46 Å (Fig. 2a), and the two crystal forms are compared in this reference frame.

The metal coordination is different in the two structures. In the Mg^{2+} form (Fig. 3a), two serines and a threonine

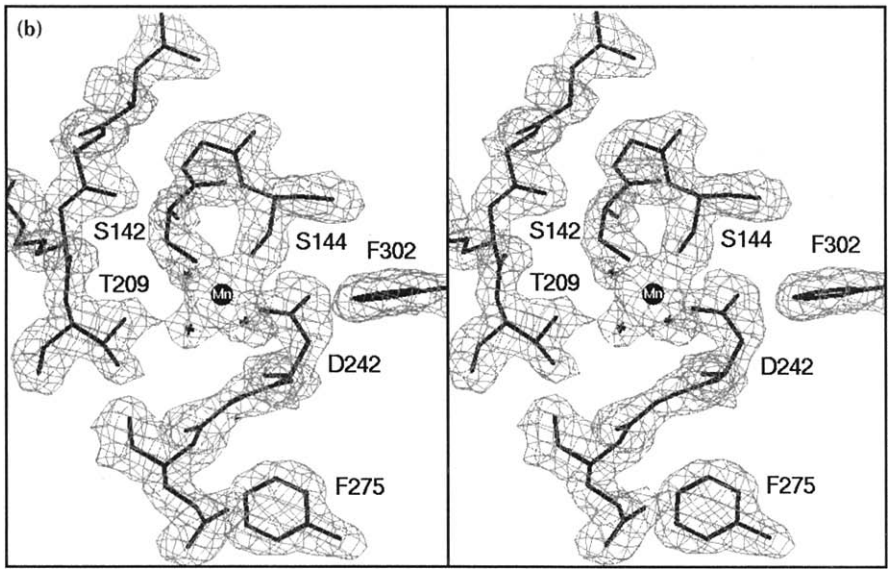

Fig. 1. **(a)** Primary sequence of the CR3 I-domain, with secondary structure assignments. Residue numbering is according to the intact protein. MIDAS residues are shown in bold. Lower-case letters denote residues invisible in the electron-density map. The last six residues are derived from the cloning vector. **(b)** Stereo electron-density map ($2F_o$–F_c) of the Mn^{2+} coordination site, contoured at 1.7σ. The two phenylalanine residues (F275 and F302) which become buried in the Mn^{2+} form are shown. Water molecules are indicated by crosses. For clarity, only density within 2 Å of the selected atoms is displayed.

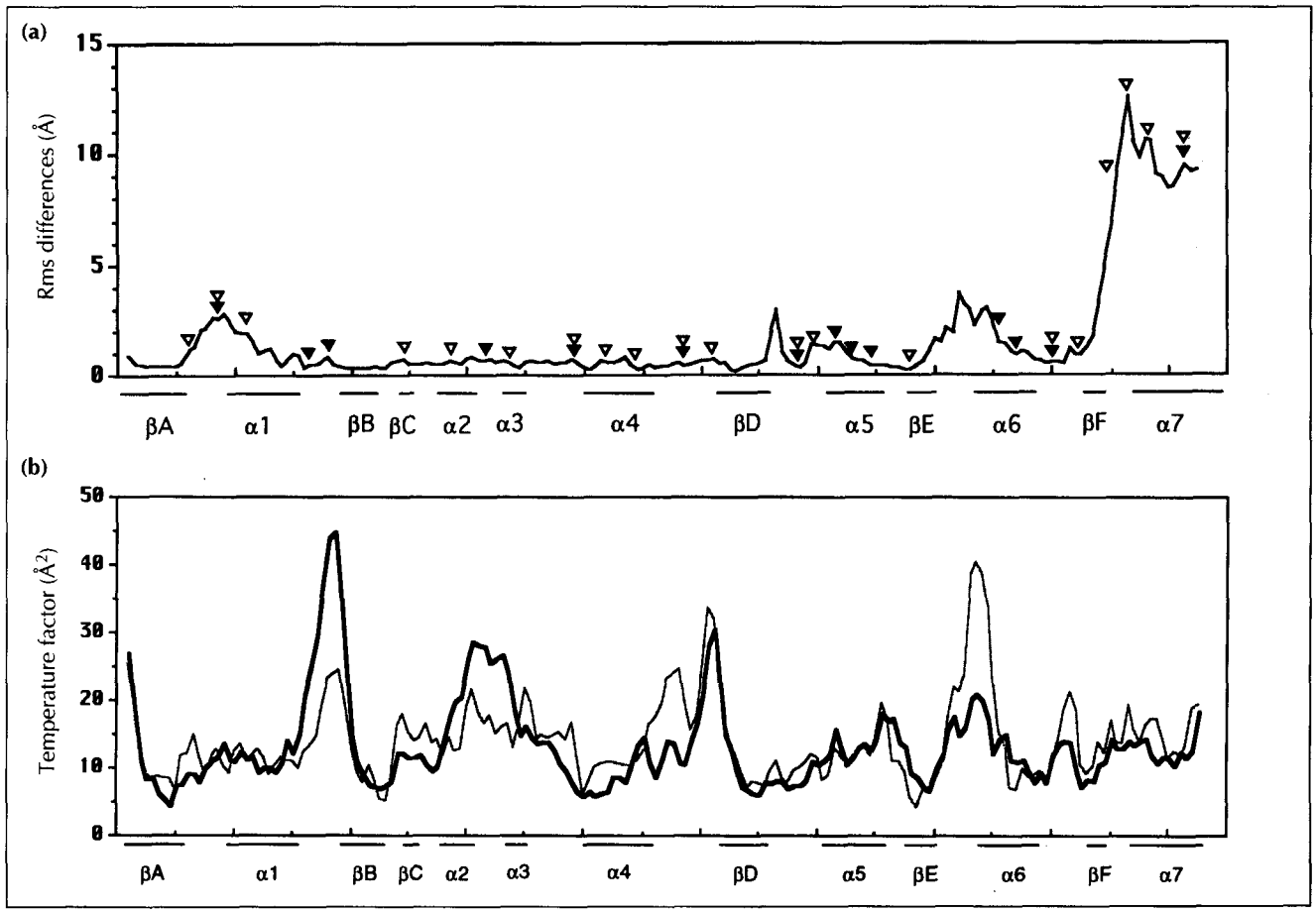

Fig. 2. **(a)** Rms difference by residue (main chain) between Mg^{2+} and Mn^{2+} I-domains. (Domains were superimposed on residues 132–140, 167–241 and 245–265 with an rms difference of 0.46 Å.) Secondary structure elements for the Mn^{2+} form are indicated along the horizontal axis. The positions of crystal contacts (interatomic distances <4 Å) for Mg^{2+} (open triangles) and Mn^{2+} (filled triangles) forms are also marked. **(b)** Comparison of main-chain temperature factors in the Mg^{2+} (thick line) and Mn^{2+} (thin line) I-domains.

make strong bonds to the metal via their side-chain hydroxyl oxygen atoms (bond lengths 2.0±0.1 Å); two water molecules also bind directly to the metal, and two aspartates make indirect contacts via water molecules. The absence of direct bonds between Mg^{2+} and the negatively charged aspartate ligands enhances the electrophilicity of the metal, and, in the crystal, the side chain of a glutamate residue from a neighbouring molecule completes the coordination; that is, the Mg^{2+} I-domain is liganded. In the Mn^{2+} form (Fig. 3b), the metal moves by 2.3 Å; bonds are made to the two serines, as before, but the bond to Thr209 is broken and replaced by a direct bond to Asp242, reducing the electrophilicity of the metal. Water molecules complete the coordination sphere, and there is no equivalent of the exogenous glutamate (the nearest acidic side chain from another molecule is 9 Å away); that is, the Mn^{2+} I-domain appears to be unliganded.

The change in metal coordination is linked to structural changes in the protein (Figs 3c,d and 4). In the Mn^{2+} form, the C-terminal helix, α7, moves 10 Å up the side of the molecule. This requires a repacking of the hydrophobic face of α7 against the side of the domain; the helix extends by an extra turn at its C terminus and bends in the middle, wrapping around the hydrophobic core. At the N terminus of α7, Phe302, which was completely exposed in the Mg^{2+} form, inserts into the top of the domain. Burial of this phenylalanine causes shifts in three loops and their connecting strands and helices which disrupt the MIDAS motif. First, the βA–α1 loop, which includes the DxSxS sequence, shifts so that Ser144 moves 1.5 Å further away from Thr209, making it impossible for a metal ion to bridge both residues. Second, the βE–α6 loop, which packed against the βA–α1 loop in the Mg^{2+} form, shifts by 1.5 Å, and rearrangements occur that bury a second phenylalanine (Phe275). Third, Phe275 packs against the βD–α5 loop, which flips so that the carbonyl of Gly243 rotates by 180° and its Cα moves by 4 Å; the Cα of Asp242 moves by 2.5 Å so that its side chain can make a direct bond to the metal.

The temperature factors (B values) are, as expected, low for the helices and strands, and higher for some of the loops, particularly the α1–βB, α4–βD and βE–α6 loops (Fig. 2b). The B values are generally well conserved between the two structures, despite the different crystal contacts and large structural changes. The C-terminal

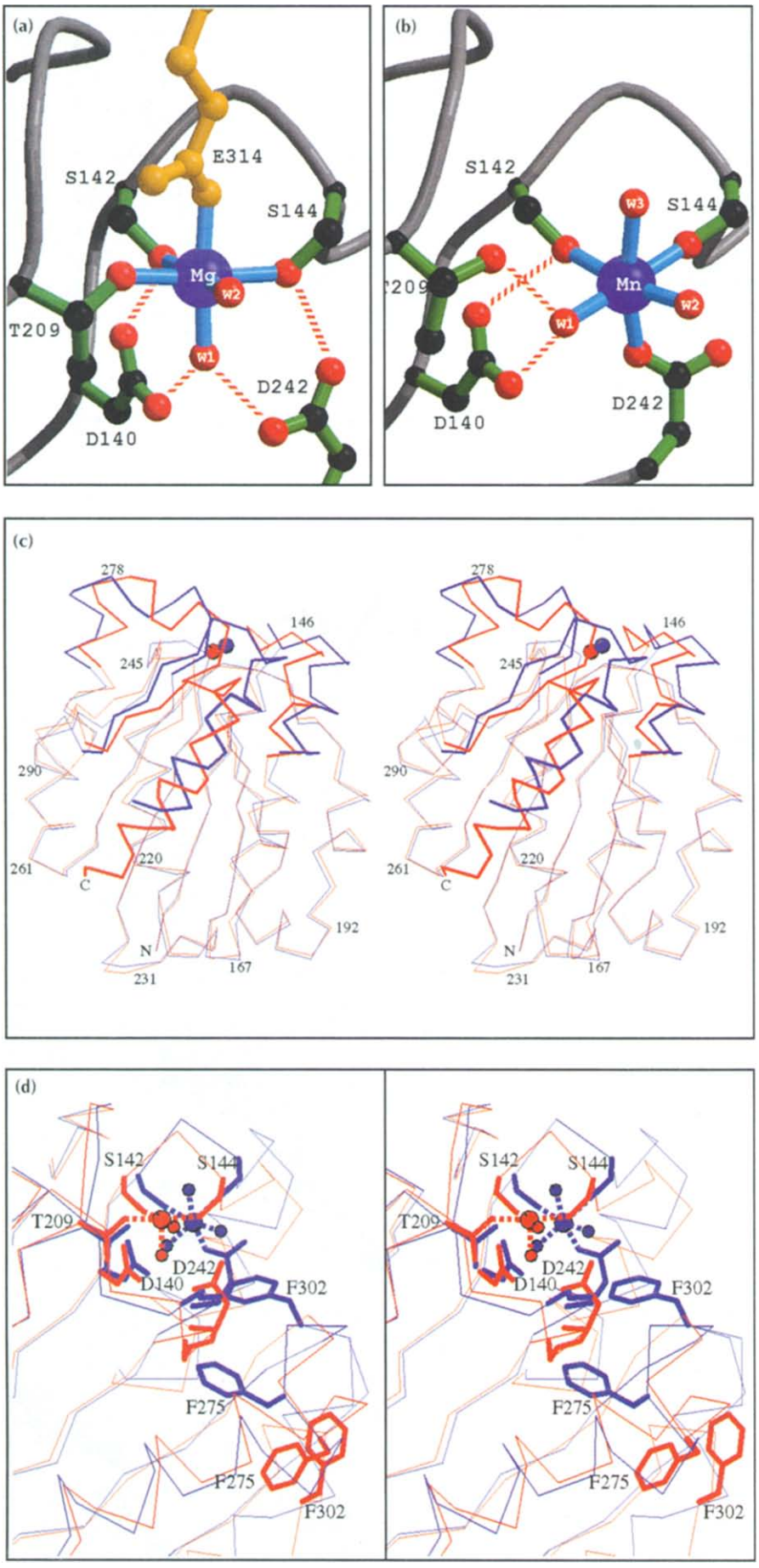

Fig. 3. Structural comparisons of the Mg^{2+} and Mn^{2+} I-domains. **(a)** The MIDAS motif in the Mg^{2+} form. **(b)** The MIDAS motif in the Mn^{2+} form. The colour code is oxygen atoms (red), carbon (black), schematic backbone (grey) and the glutamate from a neighbouring molecule (gold). Water molecules are labelled w1–w3. Selected hydrogen bonds are shown as dashed red lines. **(c)** Stereo Cα plot comparing Mg^{2+} (red) and Mn^{2+} (blue) I-domains. Regions of large change are shown with thicker lines. The metal ions are shown as spheres. The N and C termini and occasional residues are labelled. **(d)** Stereo close-up comparison of the Mg^{2+} (red) and the Mn^{2+} (blue) forms: Cα plot, together with selected side chains (metal-coordinating residues and the two buried phenylalanines), and the main chain for residues 242–243.

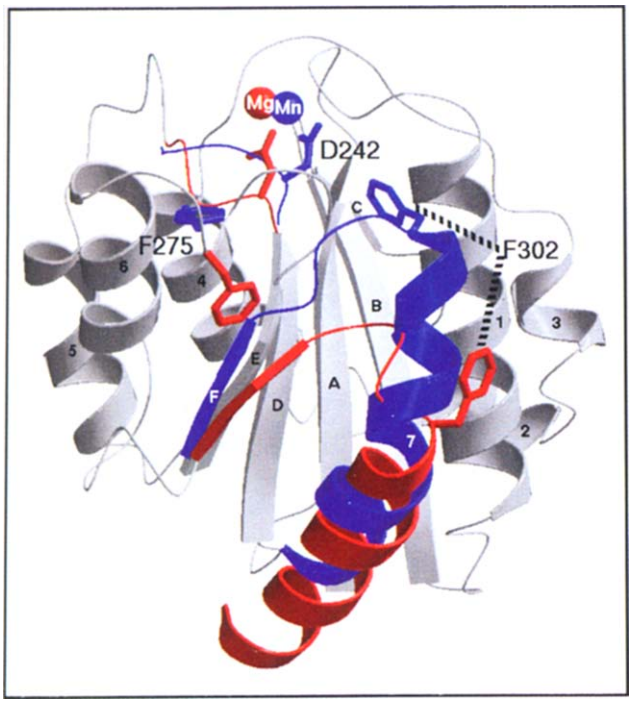

Fig. 4. Schematic diagram of the Mn^{2+} I-domain (grey). Major conformational differences are shown in red (Mg^{2+}) and blue (Mn^{2+}). β strands are labelled A–F and helices 1–7.

helix, α7, is equally well ordered in the two structures, although the βE–α6 loop is more mobile in the Mn^{2+} form. Crystal contacts are quite evenly distributed across the surface of both crystal forms (Fig. 2a). The α7 helix in the Mg^{2+} structure is involved in two major contacts centred around Phe302 and Glu314, so it is possible that crystal contacts play a role in determining the position of this helix.

Structural determinants of activation

These changes in metal coordination and associated protein movements have a striking parallel in the signal-transducing G-proteins [20–23]. For example, in the GTP-bound ('active') form of $p21^{ras}$ a Mg^{2+} ion binds directly to a serine, a threonine and two water molecules, and indirectly to an aspartate; the other coordination sites are filled by the β- and γ-phosphate oxygen atoms of the GTP. On hydrolysis of the GTP and loss of the γ-phosphate, the Mg^{2+} switches its coordination so that the bond to the threonine is lost and a direct bond to the aspartate is gained (Fig. 5). The changes in metal coordination cause large changes in the effector region which bury a previously exposed isoleucine residue and switch the molecule from an active to an inactive state. Thus, the inactive conformer of $p21^{ras}$ is characterized by reduced electrophilicity of the metal (i.e. direct coordination of an aspartate residue) and the burial of a hydrophobic residue.

Is an analogous pathway of activation operating in the I-domain? In the absence of exogenous ligand, we suggest that the Mn^{2+} form is thermodynamically favoured, owing to the burial of hydrophobic residues into the core of the protein, and that this conformation represents the inactive state. In the Mg^{2+} crystals, ligand binding (in this case provided by another I-domain molecule) and the formation of a strong bond to Thr209 provide enough energy to expel two phenylalanines from the hydrophobic core, and we suggest that this structure represents the active state. The existence of two distinct conformations is consistent with the ability of certain antibodies (that recognize epitopes on the I-domain) to discriminate between active and inactive states of the integrin [14–16]. Furthermore, the large shift of the C-terminal helix in the context of the whole integrin may radically alter the accessibility of the domain to both antibodies and protein ligands. Recent studies have shown that the ligand-binding surface is not limited to the MIDAS motif, but extends across the upper surface of the domain ([24]; P Rieu, T Sugimori and MA Arnaout, unpublished data). Indeed, the two structures have quite different surface appearances, which should provide further control of ligand affinity: for example, an acidic pocket evident in the Mg^{2+} form is largely obscured in the Mn^{2+} form (Fig. 6).

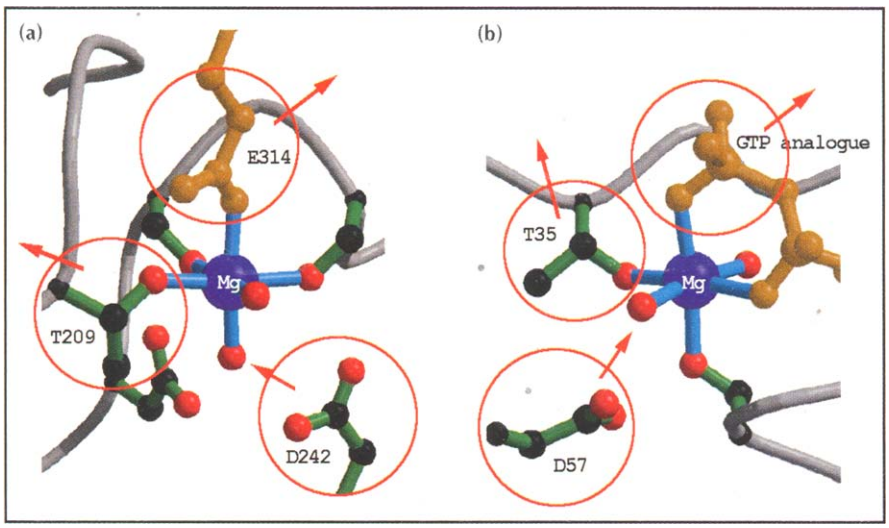

Fig. 5. Comparison of structural changes in **(a)** the MIDAS motif and **(b)** the $p21^{ras}$–GTP complex. Movements of the metal-coordinating residues are indicated (see text).

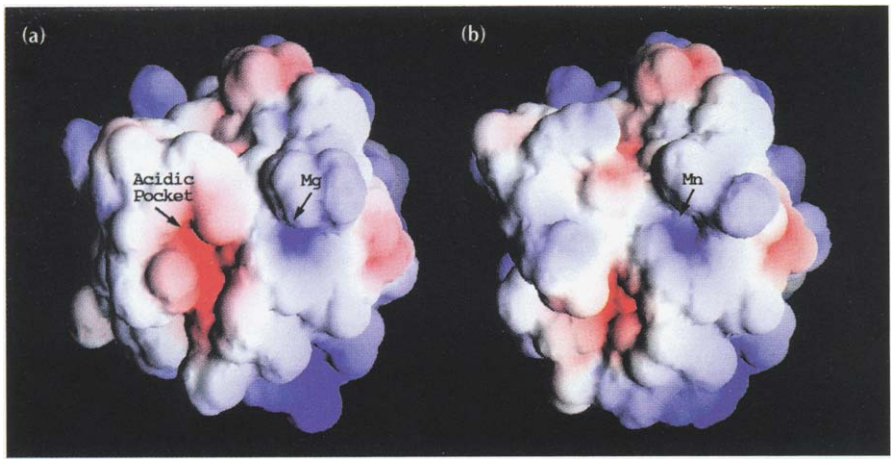

Fig. 6. Solvent-accessible surface of **(a)** the Mg^{2+} and **(b)** the Mn^{2+} I-domain, with surface charge calculated by GRASP [39]: negatively charged regions in red, positive in blue. The view is perpendicular to that shown in Figure 4.

Binding of ligands to the recombinant I-domain *in vitro* is supported by both Mn^{2+} and Mg^{2+}, but not by Ca^{2+} [9,25], recapitulating the behaviour of the intact integrin [8,26]. *In vivo*, Mg^{2+} is likely to be the cation providing the integrin–ligand bridge, because of its high concentration (~1 mM) in plasma. Our model suggests why Ca^{2+} cannot support ligand binding. The chemistry of Ca^{2+} is mostly ionic and it prefers negatively charged ligands, whereas Mg^{2+} and Mn^{2+} are smaller ions with a greater tendency to form covalent bonds [27]. Mg^{2+} and Mn^{2+} can be stably coordinated by uncharged serine and threonines residues, but Ca^{2+} cannot be thus ligated. Ca^{2+} should therefore prefer, and at high concentrations stabilize, the inactive conformation, in which an aspartate is directly coordinated instead of a threonine.

Our assignment of the Mn^{2+} crystal form as the inactive conformation appears at first sight surprising, as Mn^{2+} is well known as an activator of integrins *in vitro* [28]. We cannot provide a simple explanation for the apparent crystallization of the Mn^{2+} I-domain in an inactive form, but it should be pointed out that the binding affinities of active and inactive integrins for monomeric ligands differ typically by one order of magnitude (~1.5–2 kcal mol^{-1}), so that the difference in energy between the two I-domain conformations is likely to be small compared with typical crystal lattice energies. There are differences in metal concentrations and temperature which could explain the different crystal forms (see the Materials and methods section), and we also note that in crystals of a homologous I-domain from CD11a/CD18 (LFA-1), the molecule adopts the inactive Mn^{2+} conformation described here (with the MIDAS motif unliganded), whether grown in the presence of Mg^{2+} or Mn^{2+} (our unpublished data). This shows that the metal ion is not the sole determinant of the protein conformation, and suggests that the two conformations described in this paper represent two 'snapshots' of a dynamic equilibrium existing in solution. Clearly, further biochemical studies are required to test our proposal directly.

Our structural data suggest that the I-domain can exist in two distinct tertiary forms, a high-affinity state and a low-affinity state. Because the isolated I-domain binds ligands constitutively [8], quaternary constraints must be present in the intact αβ integrin that hold the domain in the inactive state in the absence of an activation signal [29]. We do not yet know how the tertiary changes we have described are linked to the quaternary changes that occur on integrin activation, but their magnitude and character are reminiscent of those found in other well-studied allosteric systems [30].

Biological implications

Integrins are plasma membrane proteins that mediate adhesion to other cells and to components of the extracellular matrix. Integrin-mediated cell adhesion is regulated by intracellular signals that lead to conformational changes in the extracellular domains of these receptors. This property is essential both in development and in many functions of the immune system, but its structural basis is unknown. Integrins are αβ heterodimers with a generally conserved structure. The A-domain (or I-domain) is a ~190-residue extracellular fragment from the α subunit of certain integrins that has many of the ligand-binding properties of the intact receptor. Our structural studies of this domain reveal two distinct conformations, in which a change in metal coordination is linked to large conformational changes in the protein. These changes cause a dramatic alteration in the surface of the protein implicated in binding ligand, suggesting that they are linked to a change in adhesiveness. The two conformations described here have parallels with those observed in the signal-transducing G-proteins, and we propose, by analogy, that they represent the structure of the I-domain in the active and inactive states of the integrin.

In integrins that do not contain an α subunit I-domain, a conserved region in the β subunit has been implicated in ligand binding and activation [4]. The region contains part of the metal-binding consensus sequence (DxSxS), and we have previously proposed, based on hydropathy plots, that this conserved region also adopts an I-domain

fold [17]. If this is the case, then it too may undergo structural transformations of the kind described here.

The extensive biochemical data on integrins indicate that these cell-adhesion molecules exist primarily in one of two states: active and inactive. Our results show that the I-domain can exist in two distinct tertiary states, and it is tempting to suggest a two-state allosteric model of integrin activation [31]. In such a model, the integrin is in equilibrium between a low-affinity quaternary state (inactive, 'T' state) and a high-affinity quaternary state (active, 'R' state). The T state is more stable in the absence of ligand or activation signal (owing to the burial of hydrophobic groups), but the R state has a higher affinity for ligand (owing to increased electrophilicity of the metal and the presence of a complementary ligand-binding surface). The tertiary and quaternary states are linked, so that each quaternary state is associated with a unique set of stable tertiary states, 't' and 'r'. What are the available data? First, binding of monoclonal antibodies to regions of the α or β subunit not directly involved in binding ligand can activate integrins [4]. In a two-state model, these antibodies preferentially bind to and stabilize the 'r' tertiary state of an integrin domain (i.e. the conformation of that domain in the R quaternary state), which shifts the quaternary equilibrium towards the R state, in which the tertiary state of the ligand-binding domain is in the high-affinity 'r' conformation. Second, mutations in subunits that are not directly implicated in ligand binding can have dramatic effects on integrin–ligand interactions. For example, a point mutation in the conserved region of the β subunit abolishes adhesion to physiological ligands, even though the major binding site for these ligands is located on the α subunit [32,33]. In a two-state model, the mutation locks the β-conserved region into the 't' state and thus shifts the quaternary equilibrium of the integrin towards the T state, in which the α subunit I-domain is in the 't' conformation. Finally, the exquisite sensitivity of integrins to even conservative mutations [34] is reminiscent of other well-studied allosteric systems, where point mutations can radically alter the equilibrium between the T and R states [30].

Materials and methods

Crystallization

Recombinant CD11b I-domain was expressed and purified as described previously [17]. Crystals of the Mn^{2+} form grow overnight by sitting-drop vapour-equilibration of protein (12 mg ml^{-1}) against 14% PEG 3350, 0.1 M Tris pH 8.5, 10 mM β-mercaptoethanol, 1 mM $MnCl_2$ (initial) at 4°C. Crystals grow in the monoclinic space group C2, with a=135 Å, b=37.1 Å, c=38.5 Å, β=92.6°. Under the alkaline conditions used, most of the unchelated Mn^{2+} oxidizes and precipitates (as MnO_2) within a few hours. The final concentration of Mn^{2+} ion in the crystallization drop was estimated with the dye Eriochrome Black T (Sigma Chemical Co., St Louis, MO), and found to be equimolar with the protein; rinsing the crystals in fresh Mn^{2+} solution prior to data collection ensured full metal occupancy. Most other metals, with the exception of Mg^{2+}, are unstable or precipitate under the alkaline conditions required for crystal growth. Crystals of the Mg^{2+} form grow under very similar conditions: 12% PEG 8000, 0.1 M Tris pH 8.5, 1 mM $MgCl_2$, 10 mM β-mercaptoethanol at room temperature, and belong to the tetragonal space group $P4_3$ with unit cell dimensions a=45.7 Å, c=94.3 Å [17]. Crystals do not grow in the absence of metal.

Data collection and refinement

A Mn^{2+} I-domain crystal was transferred briefly into a freshly prepared solution containing 14% PEG 3350, 0.1 M Tris pH 8.5, 1 mM $MnCl_2$, 30% glycerol, and immediately frozen in a nitrogen stream at 100 K prior to data collection. Data were collected to 2.0 Å resolution on beam line X12C of the National Synchrotron Light Source at the Brookhaven National Laboratory using a MarResearch imaging plate, with a wavelength of 0.98 Å. Data were processed with DENZO and SCALEPACK [35] to an R_{sym} of 6% (27% in outer shell) and the data are 99.5% complete (12933 unique reflections; average redundancy 3.6). The structure was solved with the molecular replacement program AMoRe [36] using the Mg^{2+} structure as the search model [17]. The rotational and translational search gave one obvious solution with an initial R-factor of 45%. The structure was refined using X-PLOR [37] and manual model building into omit maps [38]. The metal ion was not included in the initial refinement, which converged at an R-factor of 30%. Many regions of the protein had poor or discontinuous electron density at this stage, especially around the MIDAS motif and helix α7. A peak in the F_o–F_c map at the presumed location of the metal was no stronger than a water molecule peak, but inclusion of a Mn^{2+} ion into the model dramatically improved both the electron density for the MIDAS motif and the overall appearance of the map; the new position of the helix α7 also became clear in an F_o–F_c map. After rebuilding these regions the model refined smoothly to a final R-factor of 21% (outer shell=28%) for data between 12 Å and 2.0 Å resolution ($F>2\sigma$; the final R-factor for all data is 22%). The Mn^{2+} ion refines to a reasonable B value (26 $Å^2$), consistent with full occupancy of the site, although it is considerably more mobile than the metal in the Mg^{2+} I-domain. The final model comprises all non-hydrogen atoms of residues Asp132–Ala318 and 100 water molecules, and has good geometry: rms deviations from ideality of bond lengths and bond angles of 0.017 Å and 3.0° respectively. The Ramachandran plot shows that no non-glycine main-chain dihedral angles fall in the disallowed regions; 156 residues fall in the most favoured region, 8 in additional allowed regions, and 2 in generously allowed regions. These last two residues (Ser51 and Leu80) have good electron density. No solvent correction has been applied.

Coordinates for the Mg^{2+} and Mn^{2+} I-domains have been deposited with the Brookhaven Protein Data Bank, and are available from the authors.

Acknowledgements: We thank Bob Sweet and his staff at beamline X12C of the Brookhaven National Light Source for assistance in data collection; the facility is supported by the US Department of Energy, Office of Health and Environmental Research, and by the National Science Foundation. The work was supported by the Kresge and Rippel Foundations and the National Institutes of Health.

References

1. Hynes, R.O. (1992). Integrins: versatility, modulation and signaling in cell adhesion. *Cell* **69**, 11–26.
2. Sims, P.J., Ginsberg, M.H., Plow, E.F & Shattil, S.J. (1991). Effect of platelet activation on the solution conformation of the plasma membrane glycoprotein IIb–IIIa complex. *J. Biol. Chem.* **266**, 7345–7352.
3. Calvete, J.J., Mann, K., Schafer, W., Fernandez-Lafuente, R. & Guisan, J. (1994). Proteolytic degradation of the RGD-binding conformers of human platelet integrin glycoprotein IIb/IIIa: clues for identification of regions involved in the receptor's activation. *Biochem. J.* **298**, 1–7.
4. Faull, R.J. & Ginsberg, M.H. (1995). Dynamic regulation of integrins. *Stem Cells* **13**, 38–46.
5. Diamond, M.S. & Springer, T.A. (1994). The dynamic regulation of integrin adhesiveness. *Curr. Biol.* **4**, 506–517.
6. Rieu, P. & Arnaout, M.A. (1995). Structural basis and regulation of β2 integrin interactions. In *Adhesion Molecules and the Lung.* (Ward, P. & Lenfant, C., eds), Marcel-Dekker Inc., NY, in press.
7. Du, X., *et al.*, & Ginsberg, M.H. (1993). Long range propagation of conformational changes in integrin $\alpha_{IIb}\beta_3$. *J. Biol. Chem.* **268**, 23087–23092.
8. Michishita, M., Videm, V. & Arnaout, M.A. (1993). A novel divalent cation-binding site in the A-domain of the β2 integrin CR3 (CD11b/CD18) is essential for ligand binding. *Cell* **72**, 857–867.
9. Tuckwell, D., Calderwood, D., Green, L. & Humphries, M. (1995). Integrin α2 I-domain is a binding site for collagens. *J. Cell Sci.* **108**, 1629–1637.
10. Kamata, T., Puzon, W. & Takada, Y. (1994). Identification of putative ligand binding sites within I domain of integrin alpha 2 beta 1 (VLA-2, CD49b/CD29). *J. Biol. Chem.* **269**, 9659–9663.
11. Diamond, M.S., Garcia-Aguilar, J., Bickford, J.K., Corbi, A.L. & Springer T.A. (1993). The I domain is a major recognition site on the leukocyte integrin Mac-1 (CD11b/CD18) for four distinct adhesion ligands. *J. Cell Biol.* **120**, 1031–1043.
12. Randi, A. & Hogg, N. (1994). I domain of β2 integrin lymphocyte function-associated antigen-1 contains a binding site for ligand intercellular adhesion molecule-1. *J. Biol. Chem.* **269**, 12395–12398.
13. Kern, A., Briesewitz, R., Bank, I. & Marcantonio, E.E. (1994). The role of the I domain in ligand binding of the human integrin $\alpha_1\beta_1$. *J. Biol. Chem.* **269**, 22811–22816.
14. Zhou, L., Lee, D.H., Plescia, J., Lau, C.Y. & Altieri, D.C. (1994). Differential ligand binding specificities of recombinant CD11b/CD18 integrin I-domain. *J. Biol. Chem.* **269**, 17075–17079.
15. Diamond, M.S. & Springer, T.A. (1993). A sub-population of Mac-1 (CD11b/CD18) molecules mediates neutrophil adhesion to activated endothelium through an ICAM-dependent pathway. *J. Cell Biol.* **120**, 545–556.
16. Landis, R.C., Bennet, R.I. & Hogg, N. (1993). A novel LFA-1 activation epitope maps to the I domain. *J. Cell Biol.* **120**, 1519–1527.
17. Lee, J.-O., Rieu, P., Arnaout, M.A. & Liddington, R. (1995). Crystal structure of the A-domain from the α subunit of integrin CR3 (CD11b/CD18). *Cell* **80**, 631–638.
18. Arnaout, M.A. (1990). Structure and function of the leukocyte adhesion molecules CD11/CD18. *Blood* **75**, 1037–1050.
19. Haas, T.A. & Plow, E.F. (1994). Integrin–ligand interactions: a year in review. *Curr. Opin. Cell Biol.* **6**, 656–662.
20. Pai, E.F., Krengel, U., Petsko, G.A., Goody, R.S., Kabsch, W. & Wittinghofer, A. (1990). Refined crystal structure of the triphosphate conformation of H-ras p21 at 1.35 Å resolution: implications for the mechanism of GTP hydrolysis. *EMBO J.* **9**, 2351–2359.
21. Schlichting, I., *et al.*, & Goody, R.S. (1990). Time-resolved X-ray crystallographic study of the conformational change in Ha-ras p21 protein on GTP hydrolysis. *Nature* **345**, 309–315.
22. Berchtold, H., Reshetnikova, L., Reiser, C.O., Schirmer, N.K., Sprinzl, M. & Hilgenfeld, R. (1993). Crystal structure of active elongation factor Tu reveals major domain rearrangements. *Nature* **365**, 126–132.
23. Lambright, D.G., Noel, J.P., Hamm, H.E. & Sigler, P.B. (1994). Structural determinants for the activation of the α-subunit of a heterotrimeric G protein. *Nature* **369**, 621–628.
24. Huang, C. & Springer, T.A. (1995). A binding interface on the I domain of LFA-1 required for specific interaction with ICAM-1. *J. Biol. Chem.* **270**, 19008–19016.
25. Ueda, T., Rieu, P., Brayer, J. & Arnaout, M.A. (1994). Identification of the complement iC3b binding site in the β2 integrin CR3 (CD11b/CD18). *Proc. Natl. Acad. Sci. USA* **91**, 10680–10684.
26. Dransfield, I., Cabanas, C., Craig, A. & Hogg, N. (1992). Divalent cation regulation of the function of the leukocyte integrin LFA-1. *J. Cell Biol.* **116**, 219–226.
27. Cotton, F. & Wilkinson, G. (1972). *Advanced Inorganic Chemistry.* (3rd edn), pp. 206–222, John Wiley & Sons, London.
28. Altieri, D.C. (1991). Occupancy of CD11b/CD18 (Mac-1) divalent ion binding site(s) induces leukocyte adhesion. *J. Immunol.* **147**, 1891–1898.
29. Dana, N., Fathallah, D.F. & Arnaout, M.A. (1991). Expression of a soluble and functional form of the human β2 integrin CD11b/CD18. *Proc. Natl. Acad. Sci. USA* **88**, 3106–3110.
30. Perutz, M.F. (1989). Mechanisms of cooperativity and allosteric regulation in proteins. *Q. Rev. Biophys.* **22**, 139–236.
31. Monod, J., Wyman, J. & Changeux, J.-P. (1963). Allosteric proteins and cellular control systems. *J. Mol. Biol.* **6**, 306–329.
32. Bajt, M.L., Goodman, T. & McGuire, S.L. (1995). β2 (CD18) mutations abolish ligand recognition by I domain integrins LFA-1 (αLβ2, CD11a/CD18) and Mac-1 (αMβ2, CD11b/CD18). *J. Biol. Chem.* **270**, 94–98.
33. Ueda, T., Rieu, P., Brayer, J. & Arnaout, M.A. (1994). Identification of the complement iC3b binding site in the β2 integrin CR3 (CD11b/CD18). *Proc. Natl. Acad. Sci. USA* **91**, 10680–10684.
34. Bajt, M.L., Loftus, J.C., Gawaz, M.P. & Ginsberg, M.H. (1992). Characterization of a gain of function mutation of integrin $\alpha_{IIb}\beta_3$ (platelet glycoprotein IIb-IIIa). *J. Biol. Chem.* **267**, 22211–22216.
35. Otwinowski, Z. (1993). DENZO. In *Data Collection and Processing.* (Sawyer, L., Isaacs, N. & Bailey, S., eds), pp. 80–86, SERC Daresbury Laboratory, Warrington, UK.
36. Navaza, J. (1994). AMoRe: an automated package for molecular replacement. *Acta Cryst. D* **50**, 157–163.
37. Brünger, A.T. (1992). *X-PLOR Version 3.1: A system for X-Ray Crystallography and NMR.* Yale University Press, New Haven, CT.
38. Jones, T.A. (1985). Interactive computer graphics: FRODO. *Methods Enzymol.* **115**, 157–171.
39. Nicholls, A. (1993). *GRASP: Graphical Representation and Analysis of Surface Properties.* Columbia University, New York.

Received: **30 Aug 1995**; revisions requested: **27 Sep 1995**; revisions received: **23 Oct 1995**. Accepted: **24 Oct 1995**.